

PACS numbers: 42.25.Bs, 42.82. – m

PROPAGATION CHARACTERISTICS OF SURFACE PLASMON WAVES ON Au, Ag AND Al AT OPTICAL WAVELENGTHS

Reshmi Maity, Gaurav Kumar, N.P. Maity

Department of Electronics and Communication Engineering,
Mizoram University (A Central University), Tanhril, Aizawl-796009,
Mizoram, India
E-mail: maity_niladri@rediffmail.com

In this paper the propagation characteristics of Surface Plasmon Waves (SPWs) which exists on noble metals like gold (Au), silver (Ag) and aluminium (Al) due to the formation of Surface Plasmon Polaritons (SPPs), have been evaluated theoretically and simulated with the help of MATLAB programming language. The variation of the propagation constant, the attenuation coefficient and penetration depth inside the metal and the dielectric has been evaluated. The variations of the spot size width with the propagating wavelength also have been determined for the metals. It has been found that highly conducting metals Au and Ag provide a strong confinement to the SPWs than Al at optical frequencies as the spot size width of the former is found to be nearly 10 μm less than that of the later. The comparative study reveals that metal having higher conductivity can support a more confined SPW, having a lower penetration depth than metals of lower conductivity at terahertz frequencies when its dielectric constant assumes a negative value.

Keywords: ATTENUATION COEFFICIENT, PENETRATION DEPTH, PROPAGATION CONSTANT, SPOT SIZE, SPP, SPW.

(Received 04 February 2011)

1. INTRODUCTION

In the current years there has been a growing interest of SPPs which are a surface bounded electromagnetic waves coupled to electron density oscillations, guided along metal and dielectric interfaces [1]. SPPs results in the formation of electromagnetic waves which are completely confined to the interface with the fields decaying exponentially in the two media, known as Surface Electromagnetic Waves (SEW). Recently several structures of SPPs have been widely studied [2-5]. When the metal is an ideal one it is known as Fano wave while when it is a real one, having some attenuation the SEW is better known as the SPW [6]. In the field of nano-photonics and biosensors metallic nanostructures, SPWs find wide applications as Resonance Sensing [7], Raman Spectroscopy [8], Enhanced Fluorescence and Absorption [9], Nonlinear Optics [10], Nanolithography [11]. They even find applications for on-chip switching and sensing with confinement below the diffraction limit for metal-dielectric-metal waveguides [12]. Au, Ag and Al are noble metals which show a negative dielectric constant at optical frequencies in the terahertz range. The propagation constant, the attenuation coefficient, penetration depth and the width of the spot size characterizes of the SPWs and these properties are extensively studied for the three metals

and a comparison is made between them. Among the different metals studied Au is found to be the most superior metal as it has the least attenuation constant.

2. ANALYTICAL ANALYZATION OF SEW (SINGLE INTERFACE)

A planar interface of a dielectric and metal with relative dielectric constants $\varepsilon_1 = n_1^2$ ($x > 0$) and $\varepsilon_2 = n_2^2$ ($x < 0$) supporting confined propagation, where n_1 and n_2 are the refractive indices of the two medium. The two media is assumed to be semi-infinite. The coordinate axes have been chosen so that the x axis is normal to the interface with $x = 0$ corresponding to the interface. The z axis is in the direction of propagation, and y axis lies in the interface plane. The electric field and the magnetic field equations are derived with the help of the coupled mode theory as follows [13-17].

2.1 Propagation of Transverse Electric (TE) waves

For TE waves we have two electric field components for the two different media ($q = 1, 2$) in the y direction along the plane of interface.

$$E_{qy}(x, y, t) = E_{qy}(x) \exp j(\omega t - \beta z) \quad (1)$$

Hence, the wave equation will be the form of

$$\frac{\partial^2 E_{qy}(x)}{\partial x^2} + (k_0^2 \varepsilon_q - \beta^2) E_{qy}(x) = 0 \quad (2)$$

We have,

$$E_{qy}(x) = A_q \exp(-jk_q x) + B_q \exp(jk_q x) \quad (3)$$

Where

$$k_q = \sqrt{(k_0^2 \varepsilon_q - \beta^2)} \quad (4)$$

The field amplitudes are given by A_q and B_q . The radial frequency, ω is in radians / sec and the longitudinal propagation constant β is in per μm . The fields have to decay exponentially hence the wave numbers in the two media k_q has to be imaginary, $k_q = -j|k_q|$ so, equation (3) becomes,

$$E_{qy} = \frac{A_1 \exp(-|k_1| x), x > 0}{B_2 \exp(-|k_2| x), x < 0} \quad (5)$$

Where,

$$|k_1| = \sqrt{(\beta^2 - k_0^2 \varepsilon_1)} \quad (6)$$

$$|k_2| = \sqrt{(\beta^2 - k_0^2 \varepsilon_2)} \quad (7)$$

The continuity of the tangential field components and E_{qy} at $x = 0$ gives

$$|k_1| + |k_2| = 0 \quad (8)$$

which cannot be satisfied since $k_1, k_2 > 0$. Therefore, a single interface structure between that of a metal and dielectric cannot support TE confined wave propagation.

2.2 Propagation of Transverse Magnetic (TM) waves

Similarly, for TM waves we have two magnetic field components H_{qy} for the two different media ($q = 1, 2$) in the y direction along the plane of interface.

$$H_{qy} = \frac{A_1 \exp(-|k_1|x), x > 0}{B_2 \exp(-|k_2|x), x < 0} \quad (9)$$

Then the boundary conditions at $x = 0$ gives

$$\frac{|k_1|}{\varepsilon_1} + \frac{|k_2|}{\varepsilon_2} = 0 \quad (10)$$

which can be satisfied only if $\varepsilon_1, \varepsilon_2$ have opposite signs since $k_1, k_2 > 0$.

Metals exhibit negative dielectric constants in the visible and infrared wavelength regions having frequencies in the terahertz region producing structures supporting such kind of confined propagation with their amplitude decaying exponentially with increasing distance from the boundary into the different media. We start with an ideal situation which is physically not realizable of the metal having a negative real ε and later take into consideration of the realistic situation where ε is of complex value. Such confined propagation supports the Fano waves. For the analysis following, we can assume a structure of with $\varepsilon_1 > 0$ and $\varepsilon_2 = -|\varepsilon_2|$.

2.3 Fano Waves

From Maxwell's equations the Fano field components for each region from equations (5) and (9), omitting $\exp[j(\omega t - \beta z)]$ are:

Region 1 ($x > 0$)

$$H_{1y}(x) = A_1 \exp(-|k_1|x) \quad (11)$$

$$E_{1z}(x) = jA_1 \frac{|k_1|}{\omega \varepsilon_0 \varepsilon_1} \exp(-|k_1|x) \quad (12)$$

$$E_{1z}(x) = A_1 \frac{\beta}{\omega \varepsilon_0 \varepsilon_1} \exp(-|k_1|x) \quad (13)$$

Region 2 ($x < 0$)

$$H_{2y}(x) = B_2 \exp(-|k_2|x) \quad (14)$$

$$E_{2z}(x) = -jB_2 \frac{|k_2|}{\omega \varepsilon_0 |\varepsilon_1|} \exp(-|k_2|x) \quad (15)$$

$$E_{2z}(x) = -B_2 \frac{\beta}{\omega \varepsilon_0 |\varepsilon_2|} \exp(-|k_2|x) \quad (16)$$

Although H_y is continuous at the boundary, its derivative $\partial_x(H_y)$ is discontinuous. $\varepsilon_2 = (-|\varepsilon_2|)$, hence producing a negative slope $\{-|\varepsilon_1| / (|\varepsilon_2|)\}$

$$\frac{dH_{1y}}{dx} = \left\{ \frac{-\varepsilon_1}{|\varepsilon_2|} \right\} \frac{dH_{2y}}{dx} \quad (17)$$

E_x is discontinuous with again a negative slope of $\{-|\varepsilon_2| / \varepsilon_1\}$.

$$E_{1x}(x) = - \left\{ \frac{|\varepsilon_2|}{\varepsilon_1} \right\} E_{2x}(x) \quad (18)$$

This negative slope of the discontinuity of E_x and dH_y / dx is the factor that allows the single interface to support confined optical propagation something unrealizable between two media with relative dielectric constants of the same sign. From the continuity of the tangential fields at $x = 0$, the dispersion equation for the Fano guide structure can be obtained as,

$$|k_1| = \left\{ \frac{\varepsilon_1}{|\varepsilon_2|} \right\} |k_2| \quad (19)$$

The value of β can now be found analytically,

$$\beta = k_0 \sqrt{\left(\frac{\varepsilon_1 \varepsilon_2}{\varepsilon_1 + \varepsilon_2} \right)} \quad (20)$$

The term penetration depth is the distance the field travels along the x axis before its amplitude becomes 37 % of its original value. The longer the distance the weaker the wave will be confined to the surface. The inverted propagation constant $1/|k_1|$ and $1/|k_2|$ gives the penetration depth inside the dielectric and metal respectively in μm . Typically the field is 98 % in the dielectric and 2 % in the metal. Hence this shows that almost all the power will be in the dielectric making these waves suitable for sensing. Assuming confined propagation, analytic solutions for k_1 and k_2 can also be obtained from equation (19) and (20). This gives,

$$|k_1| = k_0 \sqrt{\left(\frac{\varepsilon_1^2}{|\varepsilon_2| - \varepsilon_1} \right)} \quad (21)$$

$$|k_2| = k_0 \sqrt{\left(\frac{\varepsilon_1^2}{|\varepsilon_2| - \varepsilon_1} \right)} \quad (22)$$

2.4 Surface Plasmon Waves

SPWs represent realistic situations with non-ideal metals having a complex relative dielectric constant given by $\varepsilon_2 = \varepsilon_{2R} - j\varepsilon_{2I}$ with $\varepsilon_{2R} = (-|\varepsilon_{2R}|)$ and $\varepsilon_{2I} > 0$. Because ε_2 is now complex, hence the expression for β will be complex of the form $\beta = \beta_R - j\beta_I$ with $\beta_R, \beta_I > 0$. The real part β_R is called propagation constant and the imaginary β_I is attenuation coefficient having their numerical value in the range of per μm .

$$\beta_R = k_0 \varepsilon_1^{1/2} \left\{ \frac{(\varepsilon_{2R}^2 - \varepsilon_{2R} \varepsilon_1 + \varepsilon_1^2)}{|\varepsilon_2 + \varepsilon_1|^2} \right\}^{1/2} \quad (23)$$

$$\beta_I = \frac{1}{2} \left\{ \frac{(\varepsilon_1^2 \varepsilon_{2I})}{\beta_R} \right\} \frac{k_0^2}{|\varepsilon_2 + \varepsilon_1|^2} \quad (24)$$

with $\beta_R \gg \beta$ and $\beta_R \approx \beta$

Because of the new complex β , the new $|k_1|$ and $|k_2|$ are also complex of the form $|k_1| = |k_{1R}| - j|k_{1I}|$ and $|k_2| = |k_{2R}| - j|k_{2I}|$ with $|k_{1R}|, |k_{1I}|, |k_{2R}|, |k_{2I}|$ being the corresponding real and imaginary parts of $|k_1|$ and $|k_2|$ respectively. Again the penetration depths of the fields inside the two media are now evaluated through the real parts of $|k_1|$ and $|k_2|$ respectively. Mathematically the spot size is determined as the sum of the penetration depth's inside the dielectric and inside the metal. Hence the spot size is given by,

$$\frac{1}{|k_1|} + \frac{1}{|k_2|} = \text{spotsize} \quad (25)$$

The presence of the attenuation coefficient, represents a lossy wave that can propagate for a finite distance L along the z direction until its field intensity $\exp(-2\beta_I z)$ becomes e^{-1} . Hence,

$$z = L = (2|\beta_I|)^{-1} \quad (26)$$

It is clearly shown from equation (24) that for long wavelengths since the losses of the metal is reduced, hence β_I become smaller and the propagation distance having the value in the range of μm , longer. However, there is a price to be paid for that and this is that the penetration depth inside the dielectric increases hence the field spreads more, resulting to a less intense field.

3. ANALYTICAL ANALYZATION OF SEW (THREE LAYER STRUCTURES)

3.1 Anti-symmetric structure

The anti-structure consists of a metal core with dielectric cladding. The width of the metal core is hand its dielectric constant is $\varepsilon_2 < 0$. The dielectric constants of the cladding (ε_1 and ε_3) are both greater than zero. The Fano waves have the propagation constant in the core as,

$$|k_2| = \sqrt{(\beta^2 - k_0 |\varepsilon_2|)} \quad (27)$$

Since $\varepsilon_2 < 0$, k_2 will be imaginary giving exponential solutions inside the metal. The dispersion relationship is also obtained as,

$$\tanh(|k_2| h) \left[|k_1| |k_z| \varepsilon_z^2 + |k_2|^2 \varepsilon_z \varepsilon_1 \right] + \left[|k_1| |k_2| \varepsilon_z \varepsilon_2 + |k_2| |k_z| \varepsilon_1 \varepsilon_z \right] = 0 \quad (28)$$

3.2 Symmetric Structure

Here the two dielectrics are assumed to be of the same material hence the equation (28) splits giving the Anti-symmetric and the Symmetric Fano waves

$$\tanh\left(\frac{|k_2| h}{2}\right) = \frac{\varepsilon_1 |k_2|}{|\varepsilon_2| |k_1|} \quad (29)$$

$$\tanh\left(\frac{|k_2| h}{2}\right) = \frac{|\varepsilon_2| |k_1|}{\varepsilon_1 |k_2|} \quad (30)$$

The differences between the Fano and the SPWs are similar to that observed for the single interface case. However, what it is worth mentioning is that the anti-symmetric wave has larger attenuation coefficient than the symmetric which means it exhibits more losses. Consequently the symmetric wave has a longer propagation distance, due to the lesser losses of the metals in longer wavelengths.

4. RESULTS AND DISCUSSION

4.1 The Propagation Constant and the Attenuation Coefficient

With the help of MATLAB programming the propagation constant and the attenuation coefficient is found out from equation (23) and (24) for the metal Au, Ag, Al at the different wavelengths. The graphical plots for the variation of the propagation constant and the attenuation coefficient with the wavelength are shown in Fig. 1, 2 and 3 for Au, Ag and Al respectively.

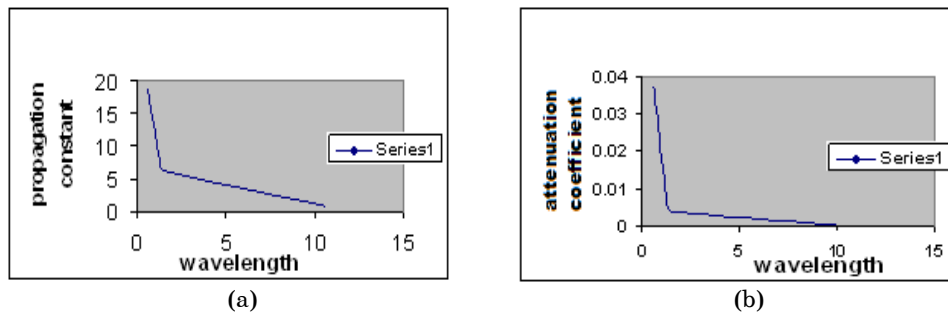


Fig. 1 – Propagation Constant (a) and Attenuation Coefficient (b) of Au

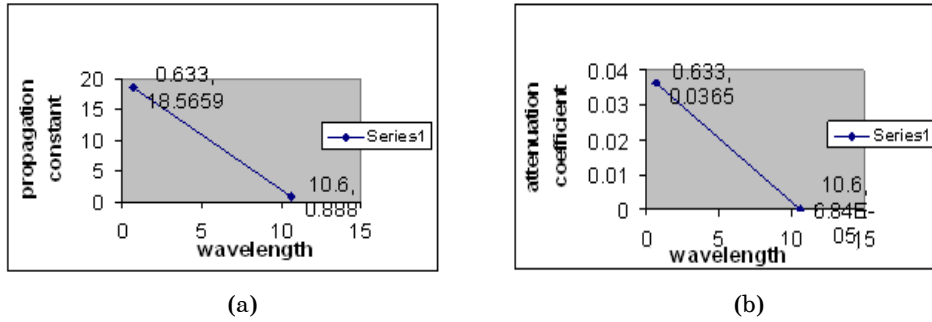


Fig. 2 – Propagation Constant (a) and Attenuation Coefficient (b) of Ag

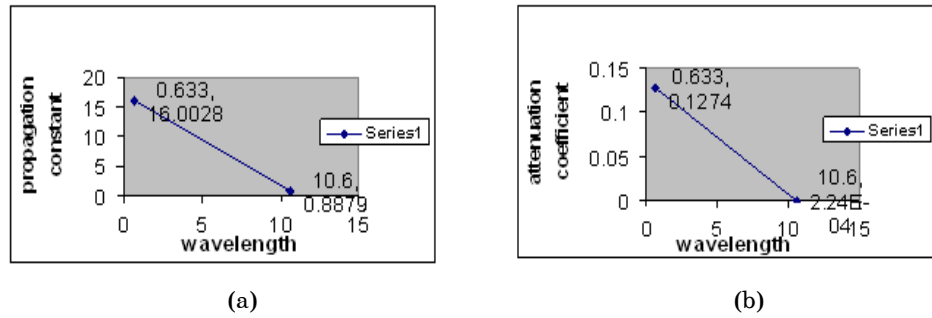


Fig. 3 – Propagation constant (a) and Attenuation coefficient (b) of Al

From the above figures we find that the propagation constant and the attenuation coefficient of Au are of higher magnitudes at higher frequencies and decreases rapidly as the frequency is decreased. Hence we have confinement of the SPWs at higher frequencies which are found out to be of the range of terahertz frequencies. Moreover the propagation constant is of lower magnitude and the attenuation coefficient is of much higher value of Al than of Ag at the same frequency of operation, hence Ag will support a more confined propagation of than of Al. The attenuation coefficient increases because of a higher value of the imaginary part of the dielectric constant of Al at the terahertz frequencies than of Ag. Therefore Au which has the highest conductivity can support SPWs more than Ag and Al.

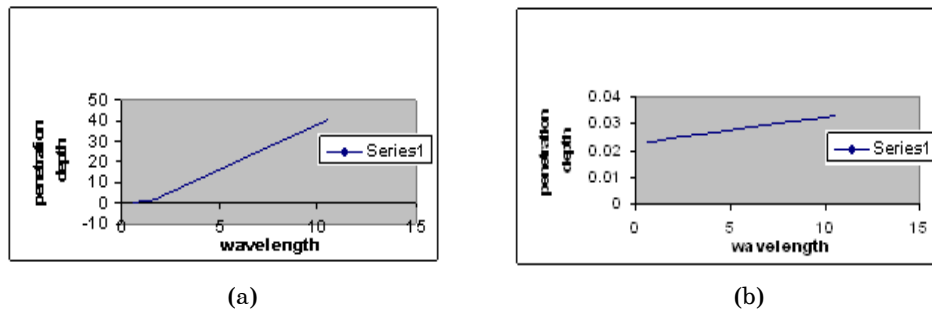


Fig. 4 – Penetration depth inside the dielectric (a) and metal (b) of Au

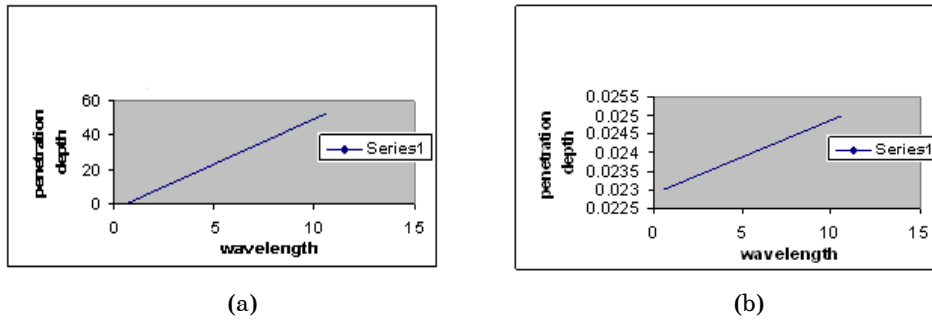


Fig. 5 – Penetration depth inside the dielectric (a) and metal (b) of Ag

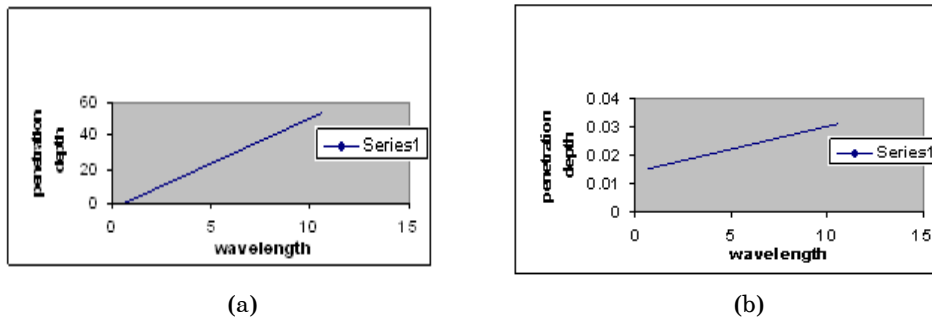


Fig. 6 – Penetration depth inside the dielectric (a) and metal (b) of Al

4.2 Evaluation of the Penetration Depth

The value of penetration depth in equation (23) and (24) is evaluated for the different metals at various wavelengths and the graphical representation of the variation with wavelength is shown in the Fig. 4, 5 and 6 for Au, Ag and Al respectively.

From the above figures it is found that the penetration depth inside the dielectric is nearly ten times more than the penetration depth inside the metal at the same frequency for Au. Since the penetration depth inside the metal is of very low magnitude hence most of the energy is confined to the surface which is essential for the propagation of the SPWs. For a three layer hetero-structure of gold – semiconductor – gold it is found that the optical gain of the core material can be made very high. The penetration depth increases with the decrease of frequency and it is maximum for Al and the least being for Ag. Increase in the penetration depth results in weak confinement of the surface plasmon waves at the surface.

4.3 Evaluation of the Spot Size

The Equation (25) is evaluated for the variation of the spot size of the different metals at various wavelengths and is shown in the Fig. 7 for Au, Ag and Al respectively.

The value of the spot size is the minimum for Au and maximum for Al. The greater the value of the spot size, the less strongly is the SPW confined to the surface as the penetration of the waves will be more in this case. Hence we again find that the more conducting materials provide a more strong confinement to the SPWs.

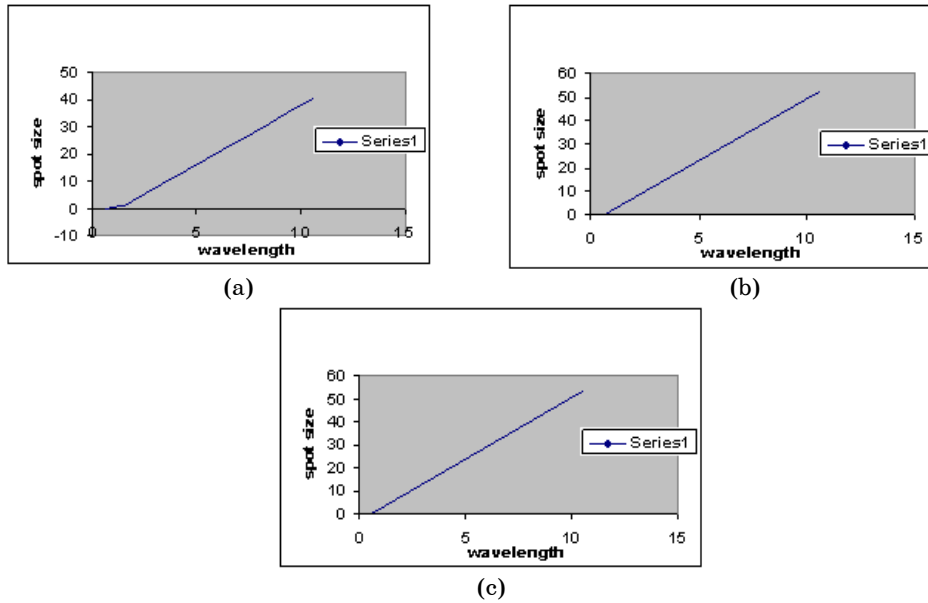


Fig. 7 – Spot size for Au (a), Ag (b) and Al (c)

4.4 Evaluation of the Propagation Distance

The value of the propagation distance is evaluated from equation (26) for the different metals at various wavelengths and is shown in the Fig. 8 for the metal Au, Ag and Al respectively.

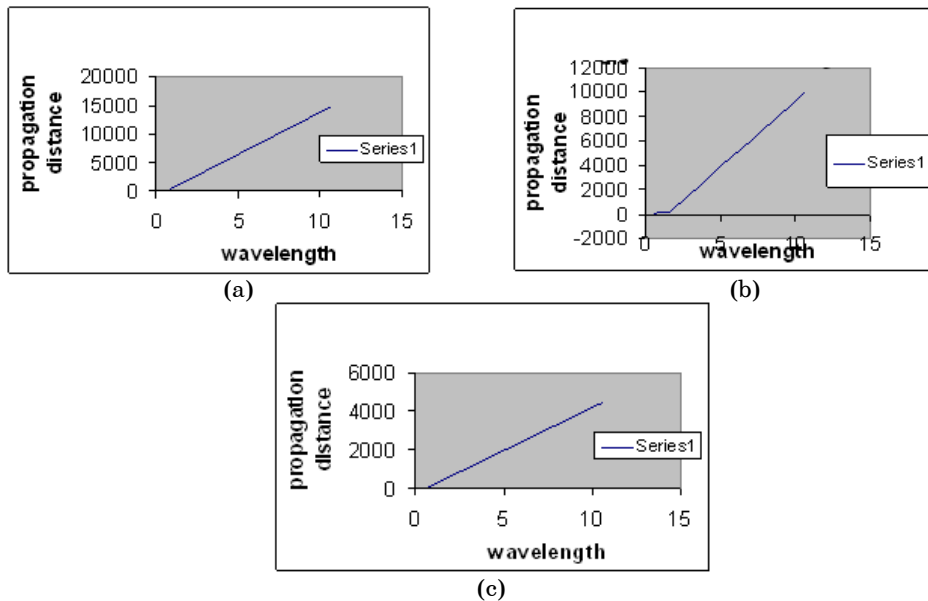


Fig. 8 – Propagation distance for Au (a), Ag (b) and Al (c)

The propagation distance for Au is 15000 μm , 10000 for Ag and only 5000 for Al at nearly the same frequency of operation. Hence much of the power of the SPW dissipates in the metal before it can travel a long distance.

4.5 The Propagation Constant for the Symmetric Three Layer Metal Core Waveguide

The propagation constant of the anti-symmetric mode of the Fano wave is evaluated with the help of equation (30) assuming $|\varepsilon_2| = 9.9$ and $\varepsilon_1 = 2.25$ at 630 nm a typical variation of β with thickness is shown in Fig. 9.

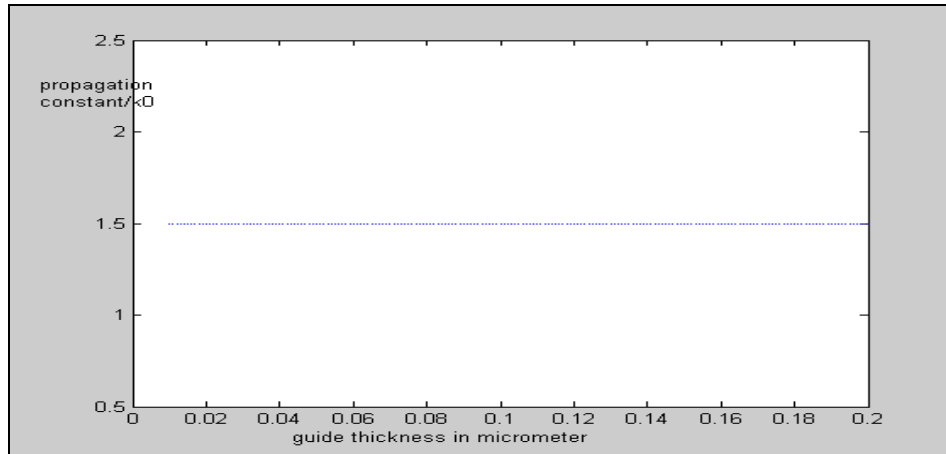


Fig. 9 – Variation of β with guide thickness

Here it is seen that there is no cut off with the guide thickness giving exponential variation with imaginary propagation constant in the metal core. An extensive study of this structure and the metal clad dielectric core structure will lead to the development of an optical microscope with resolution below the diffraction limit.

5. CONCLUSION

The study involved the variation of the propagation constant, the attenuation coefficient, the penetration depth inside the dielectric, the penetration depth inside the metal and the variation of the spot size with wavelength. Three metals, Au, Ag and Al have been considered. It is found that surface plasmon waves are highly localized since they can be excited at a single interface. This high localization of electric field is possible only at those frequencies when the dielectric constant of the metal becomes negative and it is found to be at optical frequencies. Among the different metals studied Au is found to be the most superior metal as it has the least attenuation constant. Hence as the conductivity of the metal increases the localization of the surface plasmon waves increases. This high localization results in strong field intensity, the most important feature of surface plasmon waves.

REFERENCES

1. M. Ambati, D. Genov, R. Oulton, X. Zhang, *IEEE J. Sel. Top. Quant.* **14**, 1395 (2008).
2. S. Tripathy, A. Kumar, E. Marin, J.-P. Meunier, *J. Lightwave Technol.* **28**, 2469 (2010).
3. G. Nemova, R. Kashyap, *J. Lightwave Technol.* **24**, 3789 (2010).
4. G. Nemova R. Kashyap, *Opt. Commun.* **275**, 76 (2007).
5. S. Tripathy, A. Kumar, E. Marin, J.-P. Meunier, *Appl. Optics* **48**, G53 (2009).
6. J. Burke, G. Stegeman, *Phys. Rev. B* **33**, 5186 (1986).
7. J. Homola, *Chem. Rev.* **108**, 462 (2008).
8. R. Gordon, *IEEE Nanotechnology Mag.* **12**, 12 (2008).
9. D. Schaadt, B. Feng, E. Yu, *Appl. Phys Lett.* **86**, 063106 (2005).
10. J.V. Nieuwstadt, M. Sandtke, R. Harmsen, F. Segerink, J. Prangma, S. Enoch, L. Kuipers, *Phys. Rev. Lett.* **97**, 146102 (2005).
11. N. Fang, H. Lee, C. Sun, X. Zhang, *Science* **308**, 534 (2005).
12. S. Maier, *Optics Commun.* **258**, 295 (2006).
13. M.J. Adams, *An Introduction to Optical Waveguides* (John Wiley & Sons: 1981).
14. Yariv, *Optical Electronics in Modern Communications* (Oxford University Press: 1997).
15. E. Anemogiannis, E. Glytsis, *J. Lightwave Technol.* **10**, 1344 (1992).
16. E. Sharma, M. Singh, P. Kendall, *Electron. Lett.* **27**, 408 (1991).
17. M. Ramadas, E. Garmire, A. Ghatak, K. Thyagarajan, M. Shenoy, *Opt. Lett.* **14**, 376 (1989).